Received: 16 January 2024 | Revised: 5 June 2024 | Accepted: 4 July 2024

DOI: 10.1111/cas.16290

ORIGINAL ARTICLE

Cancer Science WILEY

UBA2 SUMOylates NQO1 and promotes the proliferation of hepatocellular carcinoma by modulating the MAPK pathway

Hailong Chen[1,2] | Huifang Li[1] | Minke He[1] | Zhicheng Lai[1] | Lichang Huang[1] | Dongsheng Wen[1] | Ming Shi[1] | Anna Kan[1]

[1]Department of Hepatobiliary Oncology, Sun Yat-sen University Cancer Center, State Key Laboratory of Oncology in South China, Guangdong Provincial Clinical Research Center for Cancer, Guangzhou, People's Republic of China

[2]Department of Hepatobiliary Surgery, The Second Affiliated Hospital of Guangzhou Medical University, Guangzhou, China

Correspondence
Anna Kan and Ming Shi, Department of Hepatobiliary Oncology, Sun Yat-sen University Cancer Center, State Key Laboratory of Oncology in South China, Guangdong Provincial Clinical Research Center for Cancer, Guangzhou 510060, People's Republic of China.
Email: annakan@sysucc.org.cn and shiming@sysu.edu.cn

Funding information
National Natural Science Foundation of China, Grant/Award Number: 82072610, 82102985, 82203126 and 82272980; China Postdoctoral Science Foundation, Grant/Award Number: 2023TQ0309; National Key Research and Development of China, Grant/Award Number: 2023YFA0915700

[Correction added on 28 August 2024, after first online publication: The order of the affiliation is amended.]

Abstract

In our previous study, we found that small ubiquitin-related modifier (SUMO)-activating enzyme ubiquitin-associated-2 domain (UBA2) was upregulated in hepatocellular carcinoma (HCC) patients who were insensitive to chemoembolization. In this study, we aimed to investigate the role of UBA2 in HCC progression. Three cohorts were used to evaluate the efficacy of UBA2 as a prognostic factor for HCC. Our results indicated that UBA2 was associated with aggressive clinical behaviors and was a strong indicator of poor prognosis in HCC. In vitro experiments demonstrated that UBA2 accelerated cell growth, invasion, and migration. These results were further supported by in vivo experiments. RNA-sequencing analysis indicated NQO1 as a target of UBA2, with its levels altering following UBA2 manipulation. The results were verified by western blotting (WB) and quantitative PCR. The SUMOplot Analysis Program predicted lysine residue K240 as a modification target of UBA2, which was confirmed by immunoprecipitation (IP) assays. Subsequent mutation of NQO1 at K240 in HCC cell lines and functional assays revealed the significance of this modification. In addition, the oncogenic effect of UBA2 could be reversed by the SUMO inhibitor ML792 in vivo and in vitro. In conclusion, our study elucidated the regulatory mechanism of UBA2 in HCC and suggested that the SUMO inhibitor ML792 may be an effective combinatory treatment for patients with aberrant UBA2 expression.

KEYWORDS
LB-100, liver cancer, mitogen-activated protein kinases, ML792, small ubiquitin-related modifier

1 | INTRODUCTION

Despite considerable progress in using clinical and pathological diagnoses to predict patient survival and responses to therapy in hepatocellular carcinoma (HCC), the prognosis remains poor. Improving the classification of HCC patients could enhance the application of current treatment modalities and potentially uncover new therapeutic strategies.[1] Previously, two subclasses of HCC

Hailong Chen, Huifang Li and Minke He contributed equally to this work.

patients were identified based on significant differences in survival length. Patients with poorer survival exhibited higher expression of antiapoptotic genes and genes involved in the small ubiquitin-related modifier (SUMO) pathway.[1]

Like ubiquitin, SUMO functions by attaching to nuclear proteins as a post-translational modification.[2,3] The SUMOylation process involves an enzymatic cascade similar to the ubiquitin pathway. SUMOylation is initiated by the activation of SUMO by E1 (UBA2), followed by conjugation with E2 (Ubc9 or UBE2I). Finally, a SUMO protein is ligated to the lysine residue sidechain of a target protein, catalyzed by one of approximately 10 E3 ligases.[1,4–6] Unlike ubiquitination, SUMOylation is not associated with protein degradation but instead modifies protein activities.[3] Furthermore, the SUMO pathway significantly influences doxorubicin cytotoxicity in yeast, where mutants lacking UBA2, UBC9, ULP1, and ULP2 exhibit doxorubicin resistance.[2,7] In our previous study, we found that the expression of SUMO-activating enzyme UBA2 was upregulated in HCC patients who were insensitive to transcatheter arterial chemoembolization (TACE) treatment. Therefore, in this study, we aimed to investigate the role of UBA2 in HCC progression.

Previous reports have demonstrated the role of UBA2 in various cancer types. For instance, in over 6500 patient tumor samples across different cancer types, UBA2 expression was positively correlated with the tumor promoter EZH2.[5] Additionally, inhibition of UBA2 using ginkgolic acid could impair NOTCH1 activation in breast cancer,[3] with similar results observed in B-cell lymphoma and renal cell carcinoma.[8,9] In contrast, UBA2 was reported to be downregulated in HCC.[10] However, the underlying mechanisms of UBA2 modification in HCC remain unclear. In this study, we examined the expression of UBA2 in three independent cohorts to analyze its correlation with patient prognosis. We constructed UBA2-manipulated cell lines to investigate its effect on cell behavior and build in vivo models for further validation. Finally, proteome analysis was performed to elucidate the direct modification of UBA2 on HCC cell lines.

2 | MATERIALS AND MET1HODS

2.1 | Cell lines

The human cell lines Huh-7, SNU-368, Hep3B and SK-Hep-1 were purchased from Procell (Wuhan, China). All cell lines were characterized using short tandem repeat (STR) markers. None of these cell lines was found in the International Cell Line Authentication Committee Database of Cross contaminated or Misidentified Cell Lines (https://iclac.org/databases/cross-contaminations/). All cells were cultured in DMEM (CORNING, 10-013-CV) with 10% fetal bovine serum (FBS) and 1% penicillin/streptomycin. The cells were maintained in a humidified incubator with 5% CO_2 at 37°C. All cell lines were tested regularly for mycoplasma contamination and confirmed to be mycoplasma-free.

2.2 | Plasmid construct

All the shRNAs plasmids construct was supported by GeneCopoeia Inc., Guangzhou, China. For stable transfection experiments, human UBA2 and NQO1 were cloned into the pEZ-Lv105 vector, short hairpin RNAs (shRNA) targeting UBA2 or NQO1 were constructed into the psi-LVRU6GP vector. The FLAG-tagged NQO1 plasmid was purchased from Kidan Biosciences Co., Ltd. (Guangzhou, China). Wild-type (WT) NQO1 and its mutants were subcloned into the pCMV-MCS-3×FLAG vector. A point mutation at lysine 240 (Lys240), substituting lysine with alanine, was introduced and verified through DNA sequencing. Both WT NQO1 and its mutants were confirmed.

2.3 | Lentivirus production and infection

For lentivirus production, the Lenti-Pac™ HIV expression packaging kit (GeneCopoeia, USA) was used to produce lentiviruses in HEK293T cells. Virus-containing supernatants from HEK293T cells were collected and filtered using 0.22-μm filters. The filtered supernatant was added to 70% confluent cells in the presence of 8 μg/mL polybrene (Sigma-Aldrich, USA). After 48 h, the cells were incubated with a completely fresh medium containing the appropriate concentration of puromycin for stably transduced cells.

2.4 | RNA extraction and quantitative real-time PCR (qRT-PCR) analysis

Total RNA from cells and HCC tissues was extracted using the TRIzol reagent (Life Technologies, USA) following the manufacturers' instructions. RNA quantity was measured using a NanoDrop 2000 spectrophotometer (Thermo Fisher Scientific, USA). Total RNA was mixed with ReverTra Ace qPCR RT Master Mix with gDNA remover (TOYOBO, Japan) and reversely transcribed to cDNA according to manufacturers' instructions. qRT-PCR analysis was conducted using the THUNDERBIRD SYBR qPCR Mix (TOYOBO, Japan) and analyzed on a Bio-Rad system (Bio-Rad CFX384 Touch, USA). The results were shown as the fold change using the $2^{-\Delta\Delta CT}$ method. ACTB served as an internal control.

2.5 | Western blot

Whole-cell protein lysates were prepared using PIPA (KeyGEN, China) according to the manufacturer's instructions, and the protein concentration was quantified using the BCA assay (Thermo Fisher Scientific, USA). Cell lysates were mixed with protein loading buffer before boiling for 5 min at 95°C. Equal amounts of protein lysates were loaded and run on 7.5%–15% SDS-PAGE gels. Gels were transferred onto PVDF membranes (Bio-Rad, USA) at 250 mA for 90–150 min at 4°C. Membranes were then blocked with 5% non-fat milk

in TBST at RT for 2 h, incubated with primary antibodies overnight at 4°C and secondary antibodies at RT for 1 h, and scanned using the Bio-Rad imaging system. All experiments were performed for at least three biological repeats.

2.6 | Cell viability and proliferation assays

For the Cell Counting Kit-8 (CCK8) assay, 2000 cells were seeded into each well of 96-well plates with a complete medium. Cell viability and proliferation were evaluated using Cell Counting Kit-8 (Dojindo, Japan) every day until 7 days after seeding. Then the optical density was detected by a microplate reader at 450 and 600 nm (Bio-Tek Epoch, USA). Readouts (450–600 nm) were presented as growth curves.

2.7 | Transwell assay

The in vitro metastatic ability of cells was measured by transwell assay. Cells were serum-starved for 24 h before plating into Falcon cell culture inserts (Corning, 353097) for migration assay or premade 10% Matrigel inserts for invasion assay. Cells were re-suspended in serum-free medium and migrated/invaded into culture medium with 20% FBS. After the non-migrated/invaded cells were removed, the inserts were washed in PBS, fixed in 100% methanol, air dried, stained with 0.5% crystal violet, washed in distilled H_2O, air dried, and imaged. The migrated/invaded cells were counted using ImageJ (NIH). Fold change was calculated by the number of migrated/invaded cells relative to the control condition. For SK-Hep-1 cells, 5×10^4 cells were seeded and incubated 24 h for both migration and invasion assay. For Hep3C, Huh7, and SNU368 migration and invasion assays, 1×10^5 cells were seeded and incubated for 72 h for assays prior to fixation and quantification.

2.8 | Wound healing assay

Cells were seeded at a density of 5×10^4 cells/well into Culture-Inserts (ibidi, 80206). After 24 h, the Culture-Insert was gently removed using sterile tweezers and filled with culture medium containing 2.5% FBS. Phase-contrast images were captured at the initial time and after 96 h for SNU-368, 72 h for Hep-3B and Huh7, or 48 h for SK-Hep-1.

2.9 | In vivo experiments

In vivo experiments were performed under protocols approved by the Institutional Care and Animal Use Committee of SYSUCC.

For the subcutaneous xenograft model, UBA2- or NQO1-manipulated HCC cells (1×10^6 cells per mouse) were injected subcutaneously into the right posterior flanks of 6-week-old BALB/c nude male mice. Tumor volume based on caliper measurements was calculated using the modified ellipsoidal formula: tumor volume = 1/2 length × width^2.

For genetically engineered mouse models, hydrodynamic tail vein injection of a sterile 0.9% NaCl solution/plasmid mix containing DNA was performed. sgUBA2, sgP53, c-*myc*, and a 4:1 ratio of transposon to SB13 transposase-encoding plasmid dissolved in 2 mL of 0.9% NaCl solution and injected as 10% of the weight of each mouse in volume. Mice were injected with the 0.9% NaCl solution/plasmid mix into the lateral tail vein with a total volume corresponding to 10% of body weight in 5–7 s. Vectors for hydrodynamic delivery were produced using the Qiagen plasmid PlusMega kit. Equivalent DNA concentration between different batches of DNA was confirmed to ensure reproducibility among experiments.

2.10 | RNA-sequencing and data analysis

The RNA isolation and RNA-seq were performed following standard protocols as previously reported. In brief, RNA was extracted using the TRIzol/chloroform/phenol method. RNA-seq library was prepared by Illumina TruSeq Stranded Total RNA Gold kit using total RNA (1–3 mg per sample). RNA integrity was assessed using the RNA Nano 6000 Assay Kit of the Bioanalyzer 2100 system (Agilent Technologies, CA, USA). Sequencing was performed on the Illumina HiSeq X TEN platform (150 bp, paired end) conducted by Novogen, Beijing, China. Raw data (raw reads) in the fastq format were processed with fastp for read trimming and read-level quality control. Reads were then aligned against the human reference genome (FASTA format) using STAR (v2.7.3) under default parameters. The "rsem-calculate-expression" script of RSEM v1.3.3 was used to count the reads numbers mapped to each gene. The transcripts per million (TPM) for each gene were calculated based on the length of the gene and reads count mapped to this gene.

2.11 | Statistics

This study was approved by the Committee for the Ethical Review of Research of Sun Yat-sen University Cancer Center. Written informed consent was obtained following institutional guidelines and the declaration of Helsinki guidelines. All statistical analyses in this study were conducted using GraphPad Prism 8.0 or R 4.0. For data comparison between two experimental groups, a two-tailed *t*-test without equal variation assumption was used. For data comparison with at least three groups, one-way ANOVA analysis was first performed to assess the overall difference among groups. If differences existed, an LSD test was performed to assess the significance of differences between the two groups. Two-way repeated measures ANOVA analysis was used to assess the difference between data sets with time series measurements, including growth curves of cell proliferation

or tumor sizes. The log-rank test was used for the survival analyses for patients. *p*-values less than 0.05 were considered significant. All figures were drawn using GraphPad Prism 8.0 and R 4.0.

3 | RESULTS

3.1 | High expression of UBA2 correlates with bad patient prognosis in HCC

To study the correlation between UBA2 expression and HCC prognosis, immunohistochemical (IHC) staining was performed on specimens from a cohort of 180 HCC patients (cohort 1). The results showed that positive expression of UBA2 was primarily detected in the nucleus (Figure 1A). However, the expression levels in the tumor cell nucleus varied widely among different HCC specimens (Figure 1A, Figure S1A). Therefore, we focused on the aberrant expression of UBA2 in tumor cells. Patients were divided into two groups based on the nuclear expression of UBA2 in tumor cells: the UBA2^{high} group (positive expression in tumor cells, Figure S1B) and the UBA2^{low} group (negative expression in tumor cells, Figure S1C). The relationship between UBA2 expression in tumor cells and the clinicopathological characteristics was analyzed. Interestingly, patients in the UBA2^{high} group were significantly associated with aggressive clinicopathologic features (i.e., high serum AFP, larger tumor diameter, multiple lesions, microvascular and macrovascular invasion, and lower differentiation grade) (Table 1). These findings were confirmed by two other independent external cohorts (cohort 2, $n=163$; cohort 3, $n=206$) (Figure 1B–G).

To confirm the correlation between UBA2 expression levels in tumor cells and HCC prognoses, we compared the overall survival (OS) and disease-free survival (DFS) between the two groups. Kaplan–Meier survival analysis revealed that patients in the UBA2^{high} group had a shorter time to recurrence and worse OS and DFS than those in the UBA2^{low} group in all three cohorts (Figure 1B–G). We also compared UBA2 RNA levels using TCGA and the GTEx databases, finding that UBA2 was significantly upregulated in tumor tissues compared to normal tissue (Figure S1D,E). Additionally, UBA2 expression was higher in HCC samples with later pathological grades (Figure S1F) and advanced TNM staging (Figure S1G). To verify these results, we examined UBA2 levels in 46 pairs of matched HCC tumor-derived and non-tumor-derived specimens by quantitative real-time PCR (Figure S1H). The results showed that UBA2 expression levels were remarkably elevated in HCC tumor tissues compared with matched adjacent tissues. Moreover, UBA2 expression was significantly higher in tumor tissues from patients with advanced stages (TNM stages II and III) than in those with early-stage disease (TNM stage I) ($p<0.001$, Figure S1I).

3.2 | UBA2 promotes malignant biological behaviors in HCC

UBA2 expression in the tumor cells of HCC tissues was positively correlated with malignant clinicopathological features related to tumor metastasis such as microvascular invasion, and portal vein thrombus (Table 1). We explored the potential biological function of UBA2 in HCC cell migration and invasion. First, we examined the UBA2 expression pattern in HCC cell lines (SK-Hep-1, SNU-368, Hep3B, and Huh7, Figure 2A) and a human fetal hepatocyte line L-02. Notably, all HCC cell lines displayed significantly higher protein levels of UBA2 compared with L-02 (Figure 2A). Further investigation was conducted to determine the role of UBA2 in malignancy. SK-Hep-1 and SNU-368 were stably transfected with a UBA2 expression plasmid (pEZ-Lv201-UBA2) or a control vector (pEZ-Lv201). Comversely, a UBA2 knockdown was constructed on Hep3B and Huh7 cells. Scrambled short hairpin RNA (shRNA) was used as a negative control. The ectopic and shRNA-reduced expression of UBA2 in the cells was confirmed by western blot analyses (Figure 2B). Cell functional assays were then performed in vitro.

The results showed UBA2 knockdown in the cells significantly decelerated wound healing velocity in Hep3B and Huh7 cells (Figure 2C,D), while wound healing was more rapid in SK-Hep-1-UBA2 cells and SNU-368-UBA2 cells (Figure 2E,F). In transwell migration and invasion assays, in vitro cultured HCC cell lines were allowed to migrate through the 8-Impores of polycarbonate filters. Compared to the vector cells, UBA2 knockdown significantly decreased the migration and invasion of HCC cell lines (Figure 2G,H). Conversely, UBA2 overexpression significantly increased migration and invasion in HCC cell lines (Figure 2I,J). Additionally, UBA2 knockdown in the cells significantly inhibited foci formation (Figure 3A), whereas a higher proliferation rate was observed in UBA2-overexpressing HCC cells (Figure 3B).

In vivo assays were also performed to examine the function of UBA2 on tumorigenesis. UBA2 shRNA-transfected and scrambled shRNA-transfected HCC cells were subcutaneously injected into nude mice. Tumors from the shUBA2 group were significantly smaller than those of the control group (Figure 3C,D). This result was further validated using a hydrodynamic tumor model. TP53^{ko}/MYC^{oe}/UBA2^{ko} plasmids and an empty vector (control) were hydrodynamically injected

FIGURE 1 High expression of UBA2 indicates aggressive behavior and poor patient outcome in HCC. (A) Immunohistochemistry of UBA2 expression in an HCC patient sample, enhancing tumor and peritumor expression. (B) Kaplan–Meier survival plot analyzing UBA2 expression on overall survival (OS) in cohort 1 ($n=180$). (C) Kaplan–Meier survival plot analyzing UBA2 expression on disease-free survival (DFS) in cohort 1 ($n=180$). (D) Kaplan–Meier survival plot analyzing UBA2 expression on OS in cohort 2 ($n=163$). (E) Kaplan–Meier survival plot analyzing UBA2 expression on DFS in cohort 2 ($n=163$). (F) Kaplan–Meier survival plot analyzing UBA2 expression on OS in cohort 3 ($n=206$). (G) Kaplan–Meier survival plot analyzing UBA2 expression on DFS in cohort 3 ($n=206$).

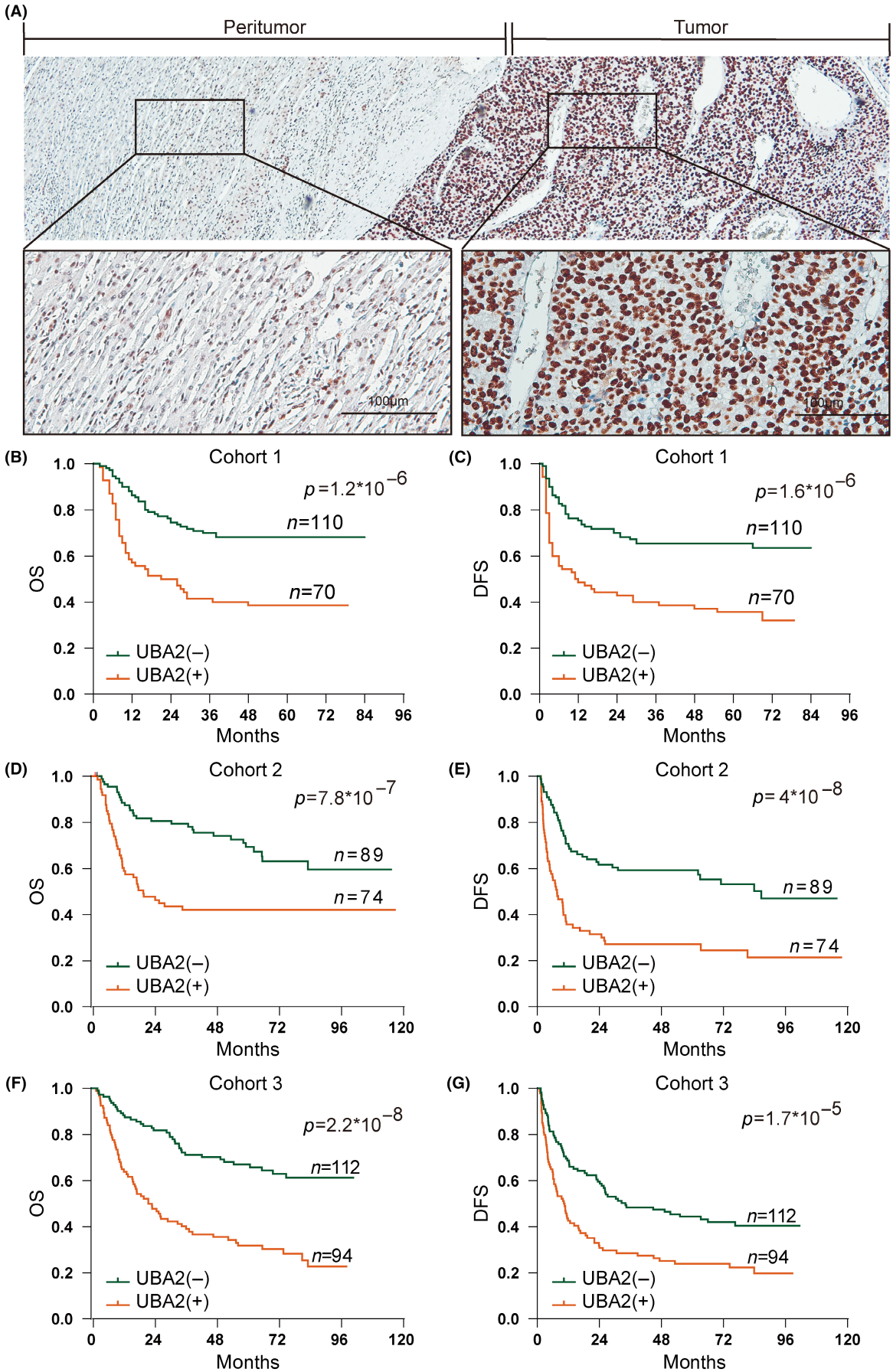
(A)
Peritumor
Tumor
100μm
100μm
(B)
Cohort 1
p=1.2*10−6
n=110
n=70
OS
UBA2(−)
UBA2(+)
Months
(C)
Cohort 1
p=1.6*10−6
n=110
n=70
DFS
UBA2(−)
UBA2(+)
Months
(D)
Cohort 2
p=7.8*10−7
n=89
n=74
OS
UBA2(−)
UBA2(+)
Months
(E)
Cohort 2
p= 4*10−8
n=89
n=74
DFS
UBA2(−)
UBA2(+)
Months
(F)
Cohort 3
p=2.2*10−8
n=112
n=94
OS
UBA2(−)
UBA2(+)
Months
(G)
Cohort 3
p=1.7*10−5
n=112
n=94
DFS
UBA2(−)
UBA2(+)
Months

into mice. The mice were monitored for abdominal mass and luciferase assay. The results showed that ablation of UBA2 significantly decelerated tumor growth in TP53^{ko}/MYC^{oe}/UBA2^{ko} mice (Figure 3E).

TABLE 1 Correlation between UBA2 expression and clinicopathologic characteristics in HCC.

Clinicopathological variables	No.	UBA2 expression levels		p
		Negative	Positive	
Age (year)				
≤49	91	57	34	0.393
>49	89	53	36	
Gender				
Female	21	12	9	0.432
Male	159	98	61	
Hepatitis B surface Ag				
Negative	16	9	7	0.434
Positive	164	101	63	
Serum AFP (ng/mL)				
<400	91	69	22	<0.001
≥400	89	41	48	
Tumor size (cm)				
≤5	119	80	39	0.015
>5	61	30	31	
Tumor number				
Solitary	133	93	40	<0.001
Multiple	47	17	30	
Microvascular invasion				
No	123	85	38	0.001
Yes	57	25	32	
PVTT				
No	156	100	56	0.032
Yes	24	10	24	
Liver cirrhosis				
No	46	29	17	0.448
Yes	134	81	53	
Differentiation grade				
I+II	108	76	32	0.002
III+IV	72	34	38	
BCLC stage				
0–A	142	94	48	0.006
B–C	38	16	22	
TNM stage				
I	86	61	25	0.007
II–IV	94	49	45	

3.3 | UBA2 modulates the mitogen-activated protein kinase (MAPK) pathway by regulating NAD(P)H quinone oxidoreductase 1 (NQO1)

To elucidate the molecular mechanism of UBA2 on the malignant behavior of HCC, RNA-sequencing was performed on UBA2 knocked down Hep3B and Huh7 cells. Gene Set Enrichment Analysis (GSEA) and GO-KEGG pathway analysis showed that MAPK-related pathways enrichment, and the regulation of MAPK pathways were downregulated in Hep-3B cells (Figure 4A,B). Additionally, a consistent downregulation of NQO1 was observed in UBA2 knocked down cells (Figure 4C,D). Given NQO1's role as a key regulator of the MAPK pathway, WB analysis was conducted, showing a significant downregulation of phosphorylated JNK, P38, and ERK1/2 in UBA2 knocked down Hep3B and Huh7 cells (Figure 4E). Conversely, in the UBA2 overexpression SK-Hep-1 and SNU-368 cells, phosphorylated JNK, P38, and ERK1/2 were upregulated (Figure 4F).

The MAPK pathway was re-analyzed after NQO1-manipulated or UBA2-manipulated HCC cells. Phosphorylated JNK, P38, and ERK1/2 were upregulated in NQO1-overexpressed cells and UBA2-downregulated cells, and downregulated in UBA2-overexpressed and NQO1-downregulated cells (Figure 5A). Given NQO1's influence on the MAPK pathway via the serine/threonine phosphatase PP2A, PP2A activity was examined in NQO1-manipulated or UBA2-manipulated HCC cells.[11] The results showed that enhanced PP2A activity in UBA2 knocked down HCC cells was inhibited by UBA2 overexpression (Figure 6D).

Functional assays were conducted to verify the effect of NQO1 on UBA2 function in HCC cells. UBA2-overexpressing Hep-3B and Huh-7 cells were transfected with NQO1 knocked down shRNA or a negative control. Our results demonstrated downregulation in the frequency of foci formation in NQO1 knocked down cells. However, upon UBA2 overexpression, migration, invasion, and foci formation rates significantly increased in vitro (Figure 5C,D). To investigate whether UBA2 knockdown could inhibit NQO1 tumorigenicity in vivo, UBA2 shRNA-transfected and scrambled shRNA transfected in NQO1-overexpressing HCC cells were subcutaneously injected into nude mice. Tumors from the shUBA2 group were significantly smaller than those from the control group (Figure 5E).

3.4 | NQO1 is modified by UBA2-mediated SUMOylation at lysine residue K240

To confirm whether NQO1 could be modified by UBA2-mediated SUMOylation, Flag-tagged NQO1 and hemagglutinin (HA)-tagged SUMO-1 and SUMO-2/3, were transfected into human embryonic kidney (HEK) 293T cells. An immunoprecipitation (IP) assay revealed

FIGURE 2 UBA2 enhances HCC invasion and migration in in vitro experiments. (A) Western-blotting analysis of UBA2 on HCC cell lines. (B) Western-blotting analysis of UBA2 on UBA2-manipulated HCC cell lines. (C, D) Wound healing assays on UBA2-knockdown HCC cell lines. (E, F) Wound healing assays on UBA2-overexpressing HCC cell lines. (G) Migration assays on UBA2-knockdown HCC cell lines. (H) Invasion assays on UBA2-knockdown HCC cell lines. (I) Migration assays on UBA2-overexpressing HCC cell lines. (J) Invasion assays on UBA2-overexpressing HCC cell lines. $^{*}p<0.05$, $^{**}p<0.01$, $^{***}p<0.001$, $^{****}p<0.0001$.

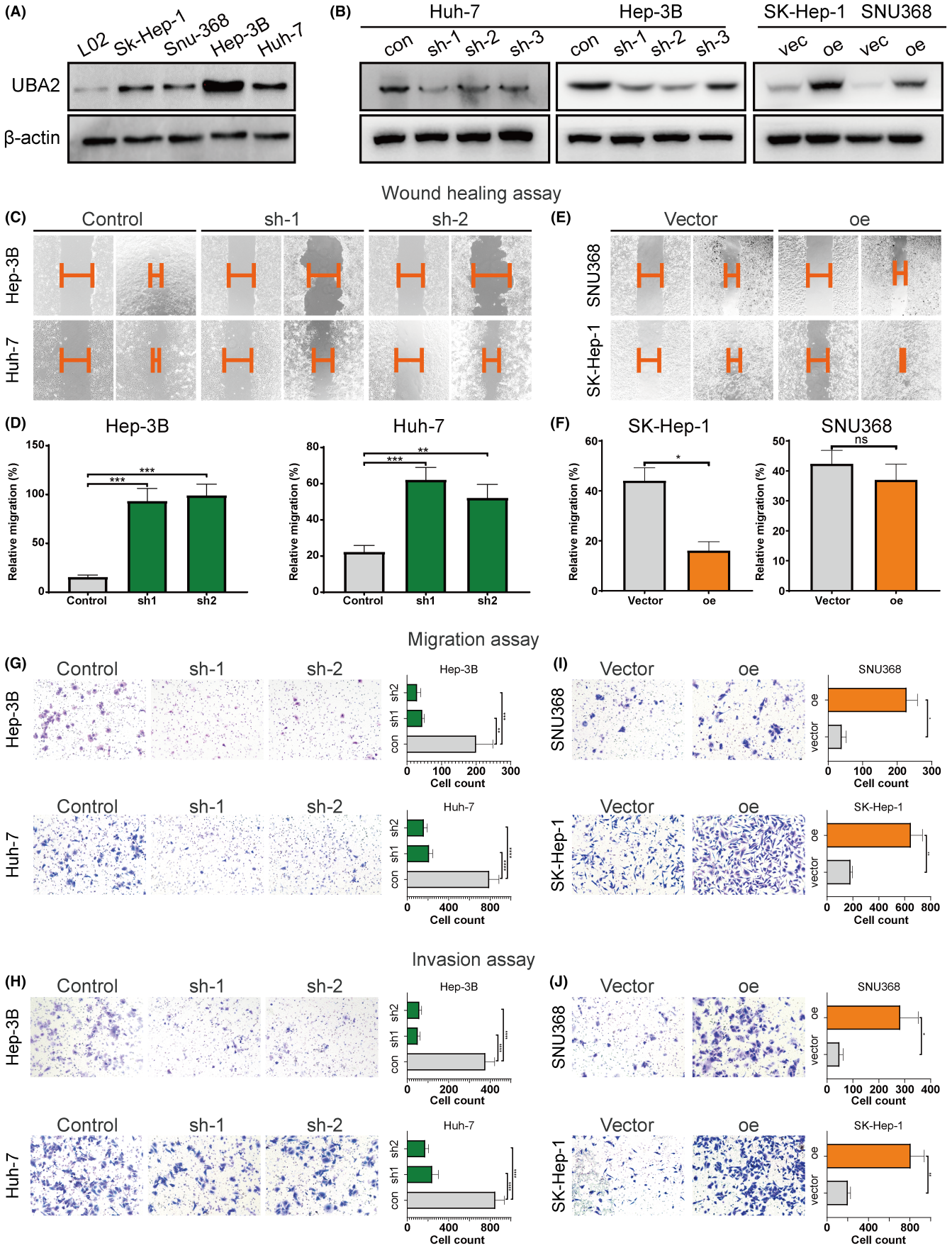
(A)
L02
Sk-Hep-1
Snu-368
Hep-3B
Huh-7
UBA2
β-actin
(B)
Huh-7
con
sh-1
sh-2
sh-3
Hep-3B
con
sh-1
sh-2
sh-3
SK-Hep-1
SNU368
vec
oe
vec
oe
Wound healing assay
(C)
Control
sh-1
sh-2
Hep-3B
Huh-7
(E)
Vector
oe
SNU368
SK-Hep-1
(D)
Hep-3B
Huh-7
Relative migration (%)
Control
sh1
sh2
(F)
SK-Hep-1
SNU368
Relative migration (%)
Vector
oe
ns
Migration assay
(G)
Control
sh-1
sh-2
Hep-3B
Huh-7
con
sh1
sh2
Cell count
(I)
Vector
oe
SNU368
SK-Hep-1
vector
oe
Cell count
Invasion assay
(H)
Control
sh-1
sh-2
Hep-3B
Huh-7
Cell count
(J)
Vector
oe
SNU368
SK-Hep-1
Cell count

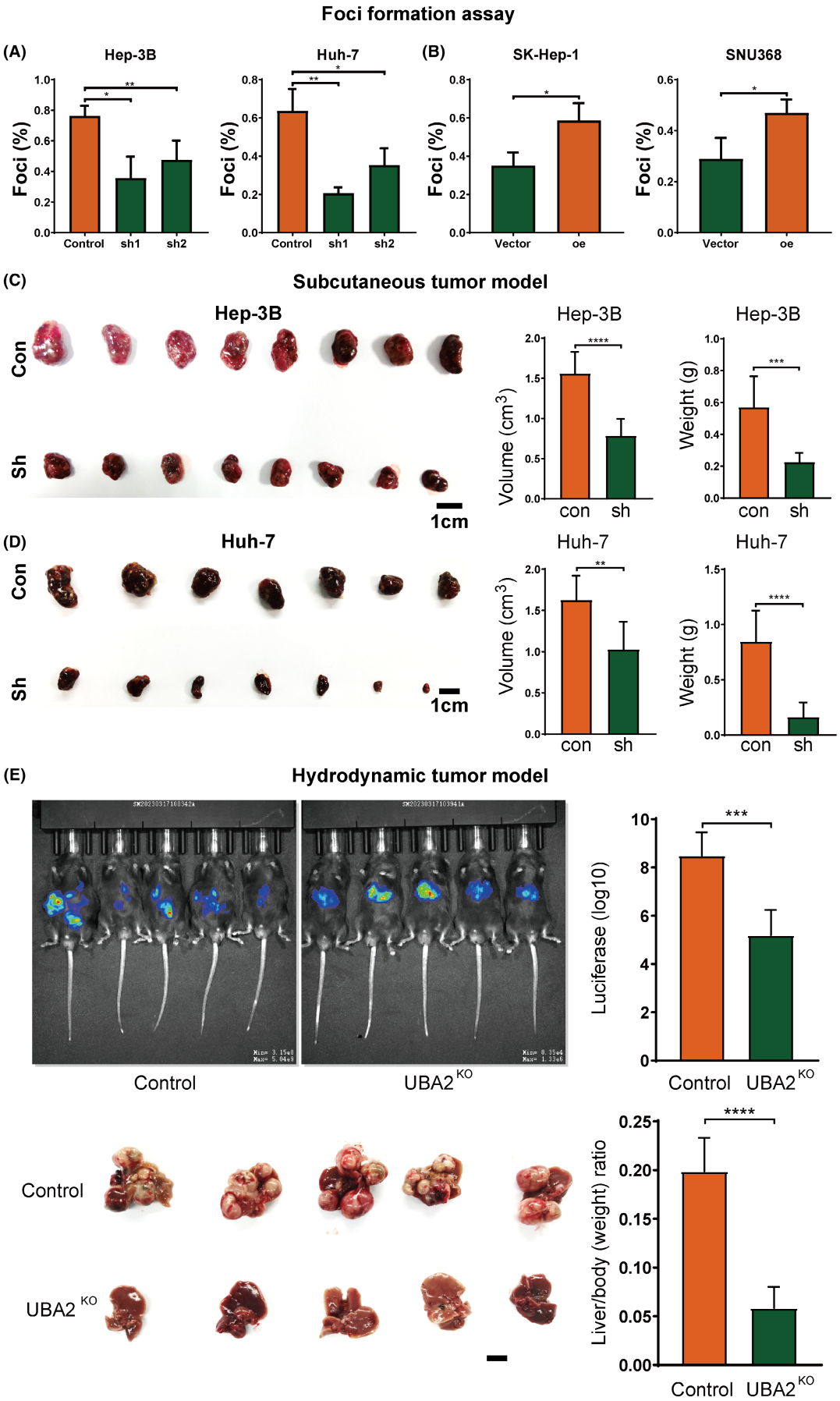
Foci formation assay
(A)
Hep-3B
Huh-7
(B)
SK-Hep-1
SNU368
Foci (%)
Control
sh1
sh2
Vector
oe
(C)
Subcutaneous tumor model
Hep-3B
Con
Sh
1cm
Volume (cm3)
Weight (g)
con
sh
(D)
Huh-7
(E)
Hydrodynamic tumor model
Control
UBA2 KO
Luciferase (log10)
Liver/body (weight) ratio

FIGURE 3 UBA2 enhances HCC growth in in vitro and in vivo experiments. (A) Foci formation assays on UBA2-knockdown HCC cell lines. (B) Foci formation assays on UBA2-overexpressing HCC cell lines. (C, D) Subcutaneous tumor models formed with UBA2-knockdown HCC cell lines (Hep-3B, $n=16$; Huh-7, $n=14$). (E) Hydrodynamic HCC mouse model formed by vector or UBA2 knocked down plasmids ($n=10$). $^{*}p<0.05$, $^{**}p<0.01$, $^{***}p<0.001$, $^{****}p<0.0001$.

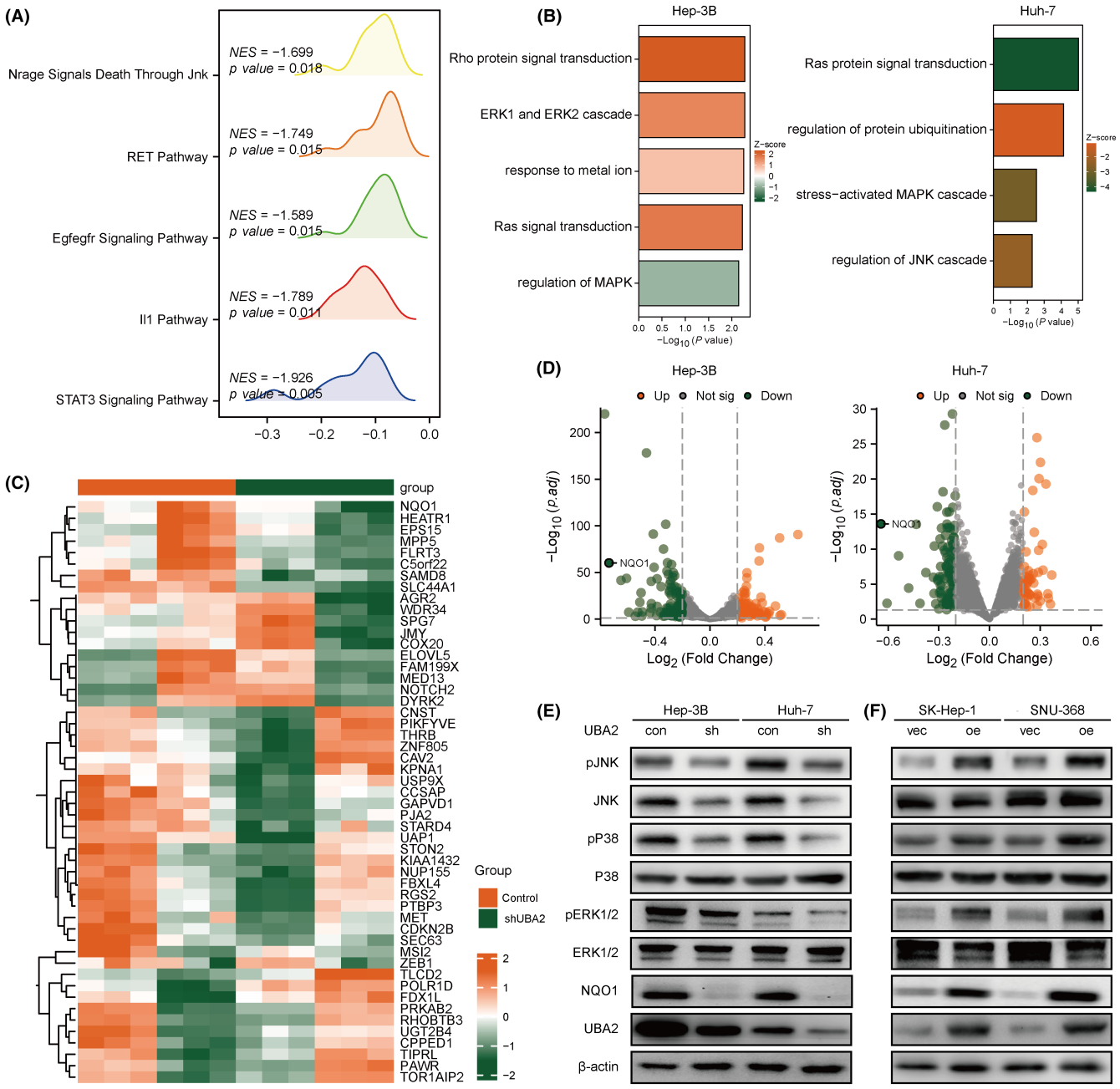

FIGURE 4 In silico analysis and proteome validation of UBA2 regulated target NQO1 and its downstream MAPK pathway. (A) GSEA analysis of UBA2-knockdown HCC cell lines. (B) GO-KEGG pathway enrichment analysis of UBA2-knockdown HCC cell lines. (C) Heat map analysis of UBA2-knockdown HCC cell lines. (D) Volcano plots of significant genes in UBA2-knockdown HCC cell lines. (E) Western-blotting analysis of the MAPK pathway in UBA2-knockdown HCC cell lines. (F) Western-blotting analysis of the MAPK pathway in UBA2-overexpressing HCC cell lines.

that NQO1 was modified strongly by SUMO2/3 and moderately by SUMO1 (Figure 6A). Subsequently, we sought to identify the SUMO modification site(s) in NQO1. Three lysine residues, K240, K91, and K61, which were predicted by the SUMOplot Analysis Program, were mutated individually to arginine for SUMOylation identification. Affinity pull-down assay showed that the mutation K240A decreased the SUMO modification levels of NQO1, while K91A and K61A showed little to no impact on NQO1 SUMOylation (Figure 6B).

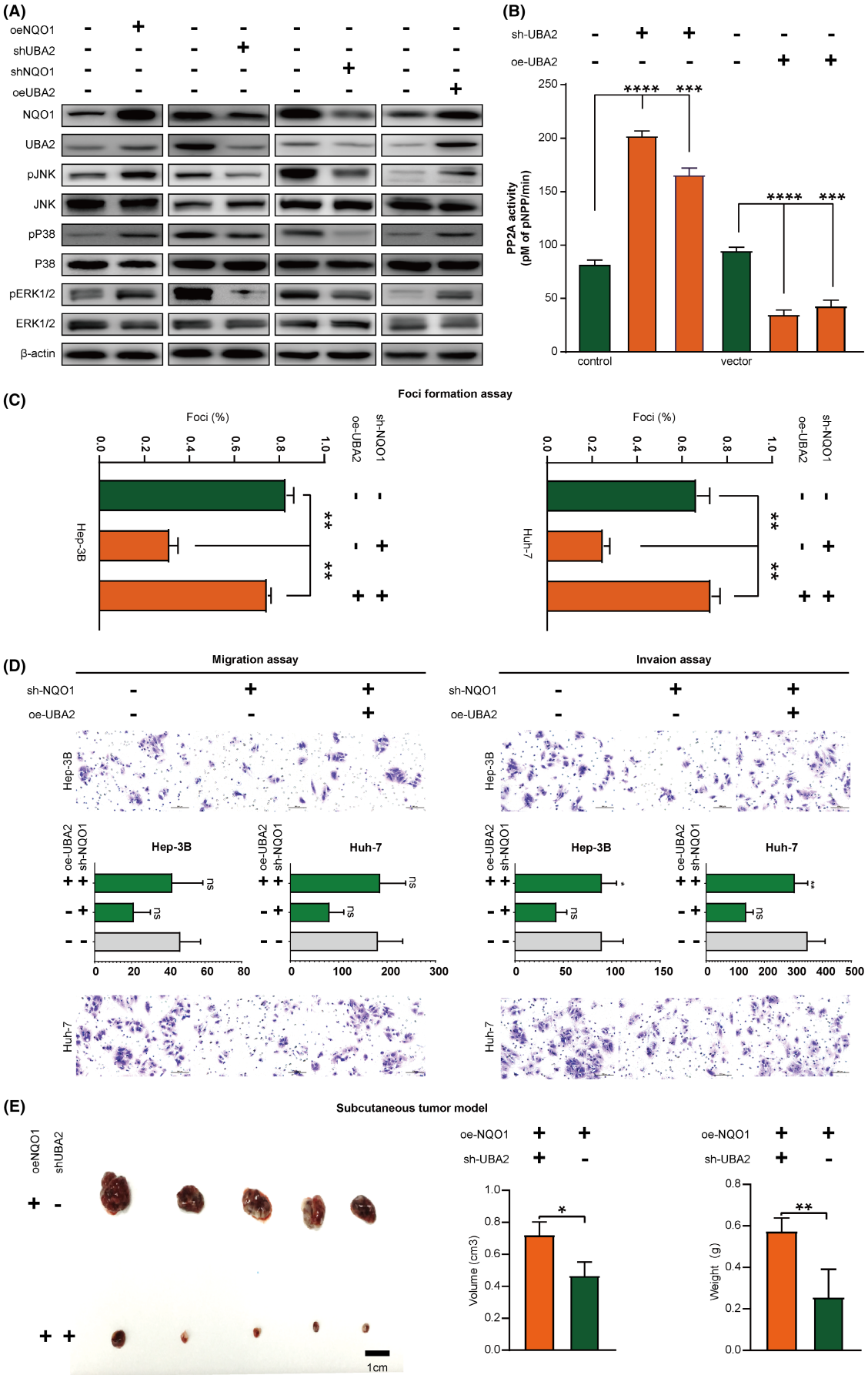
(A)
oeNQO1
shUBA2
shNQO1
oeUBA2
NQO1
UBA2
pJNK
JNK
pP38
P38
pERK1/2
ERK1/2
β-actin
(B)
sh-UBA2
oe-UBA2
PP2A activity (pM of pNPP/min)
control
vector
(C)
Foci formation assay
Foci (%)
Hep-3B
Huh-7
sh-NQO1
oe-UBA2
(D)
Migration assay
Invaion assay
sh-NQO1
oe-UBA2
Hep-3B
Huh-7
ns
(E)
Subcutaneous tumor model
oeNQO1
shUBA2
1cm
oe-NQO1
sh-UBA2
Volume (cm3)
Weight (g)

FIGURE 5 In vitro and in vivo experiments reveal the modification of UBA2 on NQO1. (A) Western-blotting analysis of the MAPK pathway in UBA2- and/or NQO1-modified HCC cell lines. (B) PP2A activity detection in UBA2- and/or NQO1-modified HCC cell lines. (C) Foci formation assays in UBA2- and/or NQO1-modified HCC cell lines. (D) Migration and invasion assays in UBA2- and/or NQO1-modified HCC cell lines. (E) Subcutaneous tumor models formed with UBA2- and/or NQO1-manipuated HCC cell lines ($n=10$). $^{*}p<0.05$, $^{**}p<0.01$, $^{***}p<0.001$, $^{****}p<0.0001$.

We then investigated the role of UBA2 in NQO1 SUMOylation. As shown in Figure 6C–F, affinity pull-down assays showed that SUMO modification was decreased by UBA2 knockdown. Furthermore, both NQO1 SUMOylation (both SUMO1 and SUMO2/3) decreased UBA2 downregulation (Figure 6D,E). IP results confirmed that lysine residue K240 was SUMOlyted by UBA2 (Figure 6G–J). HCC cell lines were employed to replicate these findings, demonstrating that only SUMO1-NQO1 K240, but not SUMO2/3-NQO1 was modified (Figure 6K).

Functional assays were conducted using NQO1-K240 mutation HCC cell lines (Figure 7A). Additionally, a selective SUMO inhibitor ML792 and PP2A inhibitor LB-100 were utilized to inhibit UBA2 function. UBA2 knockdown and LB-100 stimulation protein phosphatase 2A (PP2A) activity to determine phosphorylation activities in HCC cells after UBA2 modification. Our results indicated increased PP2A activity after UBA2 knockdown, gradually decreasing with increasing LB-100 concentration (Figure 7B). A migration and invasion assay of NQO1-K240 mutation HCC cell lines showed deceleration compared with wild-type or vector HCC cells (Figure 7C). In addition, after ML792 treatment, foci formation could be hardly detected in vitro (Figure 7D). In vivo models were then utilized for validation. UBA2-overexpressing HCC cells were subcutaneously injected into nude mice. Tumors from the oeUBA2 group were significantly larger than those of the control group but were reduced in size after ML-792 treatment. Conversely, LB-100 injection resulted in increased tumor volume and weight (Figure 7E).

4 | DISCUSSION

A major finding in this study is the regulation of UBA2 on NAD(P)H quinone oxidoreductase-1 (NQO1) (Figure 8). NQO1, a widely distributed FAD-dependent flavoprotein, serves multiple physiological functions through direct interactions with proteins and RNA.[12–14] Elevated expression of NQO1 has been reported to be associated with aggressive behavior in various cancer types, including HCC.[11,13–23] NQO1 acts as an upstream activator of the PI3K/Akt and MAPK/ERK signaling pathways and plays a role in metabolic adaptation.[11,24] Despite extensive research on NQO1, studies investigating its upstream regulatory mechanisms remain limited.

UBA2, an activator of SUMOylation, has been identified as an oncogene.[9,25,26] However, the precise modulatory mechanisms underlying UBA2's effects remain unclear. Our data support UBA2 as a prognostic factor in HCC that is positively correlated with invasive tumor behaviors. Through analysis of three patient cohorts, we observed that high UBA2 expression was associated with larger tumor size, greater tumor number, vascular invasion, higher recurrence rates, and shorter survival times. These clinical findings were corroborated by functional assays conducted on UBA2-modified HCC cell lines, demonstrating that UBA2 overexpression enhanced cell migration and invasion, whereas UBA2 knockdown inhibited cell growth and invasion.

Previous reports have documented UBA2 as a participant in epithelial–mesenchymal transition (EMT).[25–27] However, the specific involvement of UBA2 in the EMT process remains unclear. In our study, RNA-sequencing analysis of UBA2-modified HCC cells revealed a significant downregulation of NQO1 and enrichment of MAPK-related pathways. Proteome analyses further confirmed these findings, showing downregulation of NQO1 and MAPK pathway regulators in UBA2 knocked down cells, and upregulation in UBA2-overexpressing cells.

The MAPK pathway plays a critical role in the metastatic process as part of EMT. EMT transformation of malignant hepatocytes essentially equips mesenchymal offspring with antiapoptotic and migratory traits to resist cell death and to move toward a cytokine/chemokine-enriched microenvironment.[28,29] In addition, the MAPK signaling pathway can be induced by NQO1. Dimri et al.[11] discovered that NQO1 ablation could diminish the activation of the MAPK pathway and downregulate c-*myc*. Conversely, NQO1 overexpression downregulated PTEN, activated AKT and induced the expression of c-*myc*. Our study revealed similar changes in UBA2-modified HCC cell lines, suggesting a potential correlation between UBA2 and NQO1. Functional assays further validated this correlation, showing that NQO1 overexpression increased foci formation, whereas UBA2 knockdown or ML792 treatment inhibited foci formation. We also confirmed that UBA2 promoted NQO1 SUMOylation, with lysine residue K240 identified as the site of action for UBA2. Whereas UBA2 promoted NQO1 SUMOylation, it also accelerated the transcription of NQO1. This phenomenon is not uncommon, as mRNA and protein concentrations in cells achieve homeostasis,[30] leading to increased mRNA transcription with accelerated protein activity.

Our study also demonstrated that the SUMO inhibitor ML792 effectively inhibited the effects of UBA2, slowing tumor growth, invasion, and migration. In conclusion, our results elucidate the mechanism of UBA2, identifying NQO1 SUMO modification at lysine residue K240 by UBA2. The SUMO inhibitor ML792 has shown promise as a potential treatment for patients with aberrant UBA2 expression, highlighting its potential as a part of combination therapy.

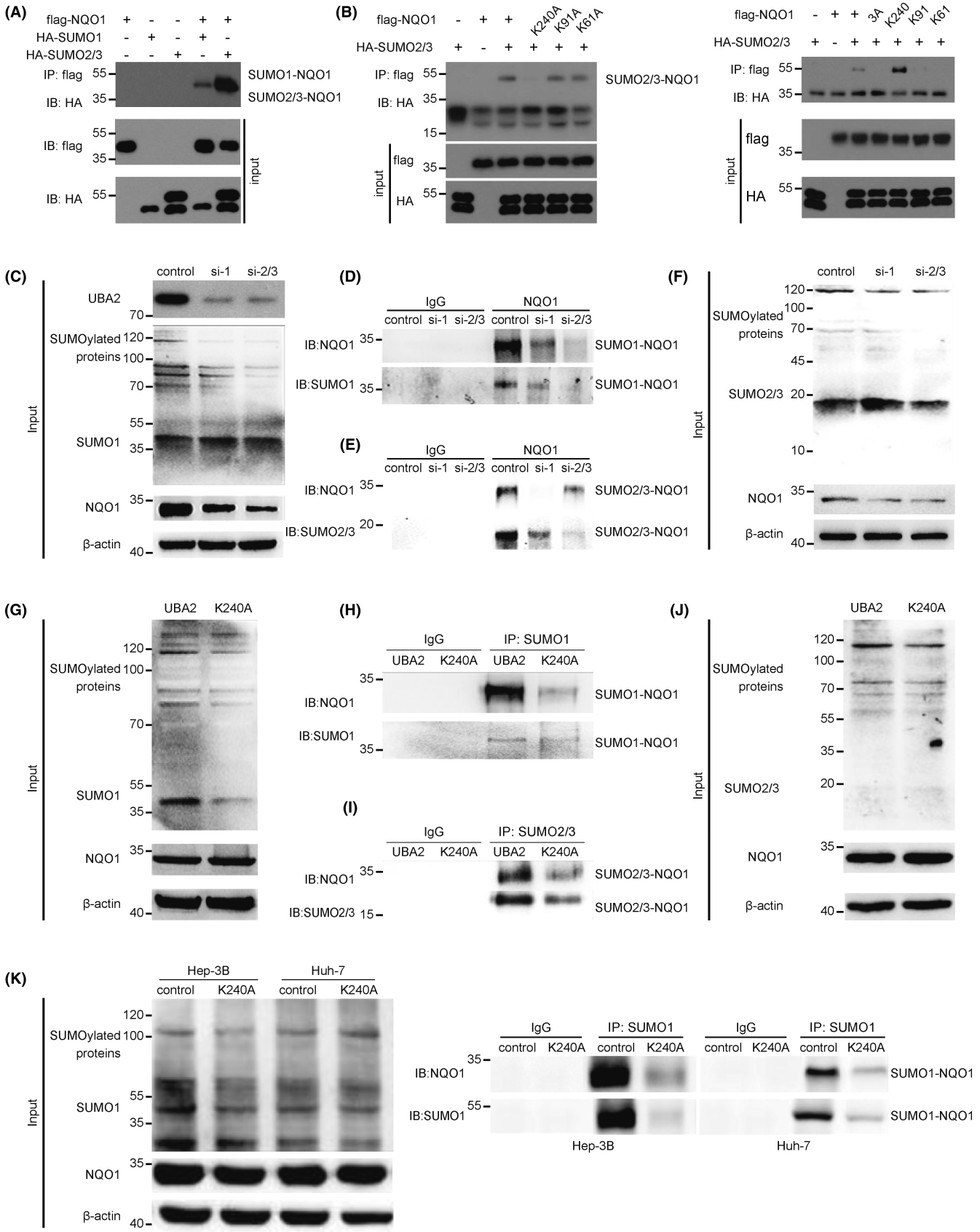

FIGURE 6 NQO1 is modified by UBA2-mediated SUMOylation at lysine residue K240. (A) Immunoprecipitation of SUMO regulators after flag-NQO1 pull-down in 293T cells. (B) Lysine residue verifications. (C, D) Immunoprecipitation of SUMO regulator SUMO1 after flag-NQO1 pull-down in UBA2 knocked down cells. (E, F) Immunoprecipitation of SUMO regulator SUMO2/3 after flag-NQO1 pull-down in UBA2 knocked down cells. (G, H) Immunoprecipitation of SUMO regulator SUMO1 in K240 mutant cells. (I, J) Immunoprecipitation of SUMO regulator SUMO2/3 in K240 mutant cells. (K) Immunoprecipitation of SUMO regulator SUMO1 in K240 mutant HCC cell lines.

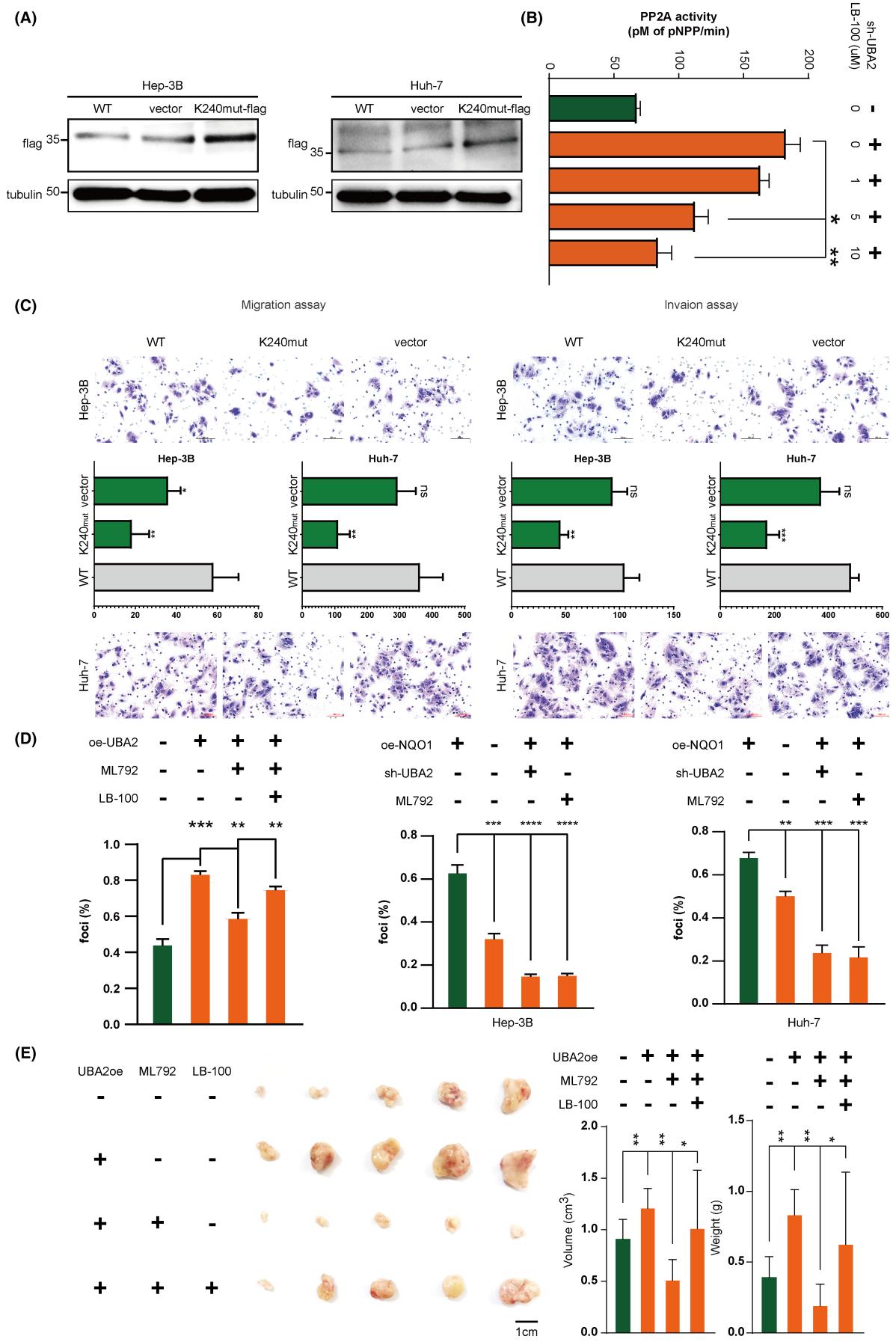
(A)
Hep-3B
WT
vector
K240mut-flag
flag 35
tubulin 50
Huh-7
WT
vector
K240mut-flag
flag 35
tubulin 50
(B)
PP2A activity
(pM of pNPP/min)
sh-UBA2
LB-100 (uM)
0
50
100
150
200
0 - 0 + 1 + 5 + 10 +
*
**
(C)
Migration assay
Invaion assay
WT
K240mut
vector
Hep-3B
Huh-7
Hep-3B
Huh-7
vector
K240mut
WT
ns
**
*
***
(D)
oe-UBA2
ML792
LB-100
oe-NQO1
sh-UBA2
ML792
foci (%)
Hep-3B
Huh-7
(E)
UBA2oe
ML792
LB-100
1cm
Volume (cm3)
Weight (g)

FIGURE 7 SUMO inhibitor ML792 and NQO1-K240 mutant can inhibit the malignant behavior of HCC. (A) Western blotting of NQO1-K240 mutation HCC cells. (B) PP2A activity detection of UBA2-knockdown HCC cells treated with PP2A inhibitor LB-100. (C) Migration and invasion assays of NQO1-K240 mutation HCC cells. (D) Foci formation assays of NQO1 or UBA2-manipulated cell lines treated with ML792 or LB-100. (E) Subcutaneous tumor models formed with UBA2-manipulated HCC cell lines treated with or without ML792 or LB-100 treatment ($n=20$). $^{*}p<0.05$, $^{**}p<0.01$, $^{***}p<0.001$, $^{****}p<0.0001$.

FIGURE 8 Schematic diagram of UBA2 SUMOylation of NQO1 and its role in promoting hepatocellular carcinoma proliferation via modulation of the MAPK pathway.

AUTHOR CONTRIBUTIONS

Hailong Chen: Conceptualization; methodology; software; validation. **Huifang Li:** Methodology. **Minke He:** Writing – review and editing. **Zhicheng Lai:** Methodology; writing – review and editing. **Lichang Huang:** Methodology; software. **Dongsheng Wen:** Methodology. **Ming Shi:** Conceptualization; visualization. **Anna Kan:** Conceptualization; methodology; supervision; writing – original draft.

ACKNOWLEDGMENTS

Appreciation is given to all patients participating in this study. We would like to express our sincere gratitude to the reviewers for their insightful comments and suggestions, which have significantly enhanced the quality of our manuscript.

FUNDING INFORMATION

This work was supported by the National Key Research and Development of China (No. 2023YFA0915700), the National Natural Science Foundation of China (No. 82272980, No. 82203126, No. 82102985, No. 82072610), and the China Postdoctoral Science Foundation (No. 2023TQ0309).

CONFLICT OF INTEREST STATEMENT

The authors declare no conflict of interest.

ETHICS STATEMENTS

Approval of the research protocol by an Institutional Review Board: N/A.

Informed Consent: N/A.

Registry and the Registration No. of the study/trial: N/A.

Animal Studies: This animal study was approved by the Medical Ethics Committee of the Sun Yat-sen University Cancer Center with procedure number L025501202205022.

ORCID

Huifang Li https://orcid.org/0009-0000-2356-9425
Ming Shi https://orcid.org/0000-0002-4051-4474
Anna Kan https://orcid.org/0000-0002-0405-6920

REFERENCES

1. Lee JS, Thorgeirsson SS. Genome-scale profiling of gene expression in hepatocellular carcinoma: classification, survival prediction, and identification of therapeutic targets. *Gastroenterology*. 2004;127(5 Suppl 1):S51-S55.
2. Huang RY, Kowalski D, Minderman H, Gandhi N, Johnson ES. Small ubiquitin-related modifier pathway is a major determinant of doxorubicin cytotoxicity in *Saccharomyces cerevisiae*. *Cancer Res*. 2007;67(2):765-772.
3. Licciardello MP, Mullner MK, Durnberger G, et al. NOTCH1 activation in breast cancer confers sensitivity to inhibition of SUMOylation. *Oncogene*. 2015;34(29):3780-3790.
4. Bossis G, Melchior F. Regulation of SUMOylation by reversible oxidation of SUMO conjugating enzymes. *Mol Cell*. 2006;21(3):349-357.
5. Du L, Fakih MG, Rosen ST, Chen Y. SUMOylation of E2F1 regulates expression of EZH2. *Cancer Res*. 2020;80(19):4212-4223.
6. Kroonen JS, Vertegaal ACO. Targeting SUMO signaling to wrestle cancer. *Trends Cancer*. 2021;7(6):496-510.
7. Seeler JS, Dejean A. SUMO and the robustness of cancer. *Nat Rev Cancer*. 2017;17(3):184-197.
8. Hoellein A, Fallahi M, Schoeffmann S, et al. Myc-induced SUMOylation is a therapeutic vulnerability for B-cell lymphoma. *Blood*. 2014;124(13):2081-2090.
9. Zhang G, Zou J, Shi J, et al. Knockdown of ubiquitin-like modifier-activating enzyme 2 promotes apoptosis of clear cell renal cell carcinoma cells. *Cell Death Dis*. 2021;12(11):1067.
10. Wong N, Chan KY, Macgregor PF, et al. Transcriptional profiling identifies gene expression changes associated with IFN-alpha tolerance in hepatitis C-related hepatocellular carcinoma cells. *Clin Cancer Res*. 2005;11(3):1319-1326.
11. Dimri M, Humphries A, Laknaur A, et al. NAD(P)H quinone dehydrogenase 1 ablation inhibits activation of the phosphoinositide 3-kinase/Akt serine/threonine kinase and mitogen-activated protein kinase/extracellular signal-regulated kinase pathways and blocks metabolic adaptation in hepatocellular carcinoma. *Hepatology*. 2020;71(2):549-568.
12. Ross D, Siegel D. The diverse functionality of NQO1 and its roles in redox control. *Redox Biol*. 2021;41:101950.
13. Fagerholm R, Hofstetter B, Tommiska J, et al. NAD(P)H:quinone oxidoreductase 1 NQO1*2 genotype (P187S) is a strong prognostic and predictive factor in breast cancer. *Nat Genet*. 2008;40(7):844-853.
14. Wang X, Liu Y, Han A, et al. The NQO1/p53/SREBP1 axis promotes hepatocellular carcinoma progression and metastasis by regulating Snail stability. *Oncogene*. 2022;41(47):5107-5120.
15. Zhan S, Lu L, Pan SS, et al. Targeting NQO1/GPX4-mediated ferroptosis by plumbagin suppresses in vitro and in vivo glioma growth. *Br J Cancer*. 2022;127(2):364-376.
16. Yang Y, Zhu G, Dong B, Piao J, Chen L, Lin Z. The NQO1/PKLR axis promotes lymph node metastasis and breast cancer progression by modulating glycolytic reprogramming. *Cancer Lett*. 2019;453:170-183.
17. Motea EA, Huang X, Singh N, et al. NQO1-dependent, tumor-selective radiosensitization of non-small cell lung cancers. *Clin Cancer Res*. 2019;25(8):2601-2609.
18. Li WY, Zhou HZ, Chen Y, et al. NAD(P)H: quinone oxidoreductase 1 overexpression in hepatocellular carcinoma potentiates apoptosis

evasion through regulating stabilization of X-linked inhibitor of apoptosis protein. *Cancer Lett*. 2019;451:156-167.
19. Lin L, Sun J, Tan Y, et al. Prognostic implication of NQO1 overexpression in hepatocellular carcinoma. *Hum Pathol*. 2017;69:31-37.
20. Chiu MM, Ko YJ, Tsou AP, Chau GY, Chau YP. Analysis of NQO1 polymorphisms and p53 protein expression in patients with hepatocellular carcinoma. *Histol Histopathol*. 2009;24(10):1223-1232.
21. Bey EA, Bentle MS, Reinicke KE, et al. An NQO1- and PARP-1-mediated cell death pathway induced in non-small-cell lung cancer cells by beta-lapachone. *Proc Natl Acad Sci U S A*. 2007;104(28):11832-11837.
22. Tada M, Yokosuka O, Fukai K, et al. Hypermethylation of NAD(P)H: quinone oxidoreductase 1 (NQO1) gene in human hepatocellular carcinoma. *J Hepatol*. 2005;42(4):511-519.
23. Kiyohara C, Yoshimasu K, Takayama K, Nakanishi Y. NQO1, MPO, and the risk of lung cancer: a HuGE review. *Genet Med*. 2005;7(7):463-478.
24. Yang Y, Zheng J, Wang M, et al. NQO1 promotes an aggressive phenotype in hepatocellular carcinoma via amplifying ERK-NRF2 signaling. *Cancer Sci*. 2021;112(2):641-654.
25. Cheng H, Sun X, Li J, He P, Liu W, Meng X. Knockdown of Uba2 inhibits colorectal cancer cell invasion and migration through downregulation of the Wnt/beta-catenin signaling pathway. *J Cell Biochem*. 2018;119(8):6914-6925.
26. Jiang B, Fan X, Zhang D, Liu H, Fan C. Identifying UBA2 as a proliferation and cell cycle regulator in lung cancer A549 cells. *J Cell Biochem*. 2019;120(8):12752-12761.
27. Zhou Q, Yin Y, Yu M, et al. GTPBP4 promotes hepatocellular carcinoma progression and metastasis via the PKM2 dependent glucose metabolism. *Redox Biol*. 2022;56:102458.
28. Giannelli G, Koudelkova P, Dituri F, Mikulits W. Role of epithelial to mesenchymal transition in hepatocellular carcinoma. *J Hepatol*. 2016;65(4):798-808.
29. Xia H, Chen J, Shi M, et al. EDIL3 is a novel regulator of epithelial-mesenchymal transition controlling early recurrence of hepatocellular carcinoma. *J Hepatol*. 2015;63(4):863-873.
30. Lin J, Amir A. Homeostasis of protein and mRNA concentrations in growing cells. *Nat Commun*. 2018;9(1):4496.

SUPPORTING INFORMATION

Additional supporting information can be found online in the Supporting Information section at the end of this article.

How to cite this article: Chen H, Li H, He M, et al. UBA2 SUMOylates NQO1 and promotes the proliferation of hepatocellular carcinoma by modulating the MAPK pathway. *Cancer Sci*. 2024;115:2998-3012. doi:10.1111/cas.16290